Photographical Record of the Dispersion Surface in Rotating Crystal Electron Diffraction Pattern

G. LEHMPFUHL and A. REISSLAND

Fritz-Haber-Institut der Max-Planck-Gesellschaft, Berlin-Dahlem *

(Z. Naturforsch. **23a**, 544—549 [1968]; received 24 January 1968)

Dedicated to Prof. P. P. EWALD *on his 80-th Birthday*

Strong interacting wave fields in a wedge-shaped crystal are separated into different plane waves when leaving the crystal and reveal points on the dispersion surface. By rotating the crystal while moving the film one obtains a photographical record of a section through the dispersion surface which may be compared with theory. An experiment with a macroscopic MgO wedge is reported. The 002 interference with excitation error nearly zero was recorded near the [$\bar{1}$10] zone axis while rotating the crystal about the [001] axis. The diagrams are compared with dynamical 17-beam calculations. The results show that a reduction of the infinite dynamical system of equations to 17 equations is correct under these special geometrical conditions.

Electron diffraction patterns from single crystals are frequently modified by dynamical n-beam effects. These phenomena are well-known from the complicated structures in convergent beam and Kikuchi diagrams near the intersection points of lines and within crossing bands as discussed in detail by many authors (e. g. [1–5]), and in the fine structure of the diffraction pattern of a crystal wedge [6, 7].

Dynamical n-beam interactions are usually classified as systematic and accidental interactions according to HOERNI [8]. In order to get a two-beam case in experiment one tries to find directions for the incident beam to avoid accidental interactions. The effect of weak simultaneous reflections can be taken into account by Bethe's second approximation. The limit of this approximation was recently investigated and discussed by HERZBERG [9]. The influence of systematic interactions, however, can become very strong for reflections with large V_g/g (V_g = structure potential, g = reciprocal lattice vector) independent of azimuth, discussed by HOWIE and WHELAN [10], GOODMAN and LEHMPFUHL [11]. Similarly, in crystals with strongly scattering atoms and large unit cell dimensions, the two-beam approximation becomes inaccurate. Furthermore, the diffraction with high voltage electrons up to 1500 – 2000 kV becomes more and more dynamic as UYEDA [12], HUMPHREYS [13], AYROLES and MAZEL [14] pointed out. It is then necessary, by use of computer methods, to investigate more complicated n-beam interactions. The advantage of an analysis of n-beam interactions is the possibility of using the information from complicated diffraction phenomena. This was demonstrated, e. g., for a determination of the phase angles of structure amplitudes by KAMBE [5], or for a refinement of structure potential determination by MOLIÈRE and WAGENFELD [6], GOODMAN and LEHMPFUHL [11] or for the evidence of Friedel's Law breakdown by UYEDA and MIYAKE [15], GOODMAN and LEHMPFUHL [16].

Theory

The diffraction of electrons in a perfect single crystal is described by BETHE's formulation [17]. For the following we refer to LEHMPFUHL and MOLIÈRE [7]. We are concerned only with elastic scattering without regard to absorption. From Schrödinger's equa-

* Abteilung Prof. Dr. K. MOLIÈRE.

1 I. ACKERMANN, Ann. Phys. Leipzig **2,** 19 [1948].
2 CHR. MENZEL-KOPP, Ann. Phys. Leipzig **6,** 259 [1951].
3 E. FUESS and E. H. WAGNER, Z. Naturforsch. **6a,** 1, 79, 133 [1951].
4 H. PFISTER, Ann. Phys. Leipzig **11,** 239 [1953].
5 K. KAMBE, J. Phys. Soc. Japan **12,** 13 [1957].
6 K. MOLIÈRE and H. WAGENFELD, Z. Kristallogr. **110,** 3 [1958].
7 G. LEHMPFUHL and K. MOLIÈRE, Z. Phys. **164,** 389 [1961].
8 I. A. HOERNI, Phys. Rev. **102,** 1534 [1956].
9 B. HERZBERG, Doctorate Thesis, Freie Universität Berlin 1968.
10 A. HOWIE and M. J. WHELAN, Proc. European Reg. Conf. Electron Microscopy, Delft 1960, p. 181.
11 P. GOODMAN and G. LEHMPFUHL, Acta Cryst. **22,** 14 [1967].
12 R. UYEDA, Acta Cryst. A **24,** 175 [1968].
13 C. J. HUMPHREYS, Anniversary Meeting on Electron Diffraction, London 1967.
14 R. AYROLES and A. MAZEL, J. Microscopie **6,** 135 [1967].
15 R. UYEDA and S. MIYAKE, Acta Cryst. **10,** 53 [1957].
16 P. GOODMAN and G. LEHMPFUHL, Acta Cryst. A **24** [1968].
17 H. BETHE, Ann. Phys. Leipzig **87,** 55 [1928].

Dieses Werk wurde im Jahr 2013 vom Verlag Zeitschrift für Naturforschung in Zusammenarbeit mit der Max-Planck-Gesellschaft zur Förderung der Wissenschaften e.V. digitalisiert und unter folgender Lizenz veröffentlicht: Creative Commons Namensnennung-Keine Bearbeitung 3.0 Deutschland Lizenz.

This work has been digitalized and published in 2013 by Verlag Zeitschrift für Naturforschung in cooperation with the Max Planck Society for the Advancement of Science under a Creative Commons Attribution-NoDerivs 3.0 Germany License.

Zum 01.01.2015 ist eine Anpassung der Lizenzbedingungen (Entfall der Creative Commons Lizenzbedingung „Keine Bearbeitung") beabsichtigt, um eine Nachnutzung auch im Rahmen zukünftiger wissenschaftlicher Nutzungsformen zu ermöglichen.

On 01.01.2015 it is planned to change the License Conditions (the removal of the Creative Commons License condition "no derivative works"). This is to allow reuse in the area of future scientific usage.

tion one derives

$$(1+\varphi_0-\boldsymbol{S}_g^2)\,\psi_g+\sum_{h\neq 0}{}'\,\varphi_h\cdot\psi_{g-h}=0\,. \qquad (1)$$

φ_g is the Fourier coefficient V_g of the potential divided by the accelerating voltage E and the $\boldsymbol{S}_g$ are the wave vectors of the crystal waves divided by the absolute value of the wave vector of the vacuum wave $|\boldsymbol{K}|=2\pi/\lambda$. The incident plane wave generates in the crystal Bloch waves being a superposition of plane waves. The wave vectors of the crystal waves are connected with the wave vector of the incident wave by the boundary conditions. These amount to the continuity of the tangential components of the wave vectors at the boundary as shown schematically in Fig. 1. $\boldsymbol{S}_e$ is a unit vector

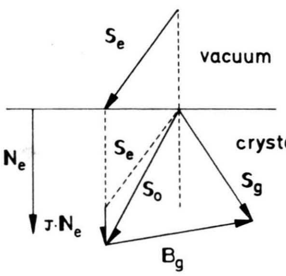

Fig. 1. Schematic diagram to show the continuity of the tangential components of the wave vectors at the boundary. $\boldsymbol{S}_e$ a unit vector in the direction of the vacuum wave. $\boldsymbol{S}_0$ and $\boldsymbol{S}_g$ wave vectors in the crystal, $\boldsymbol{B}_g$ reduced reciprocal lattice vector, $\boldsymbol{N}_e$ a vector normal to the entrance surface.

in the direction of the incident vacuum wave, $\boldsymbol{N}_e$ is a unit vector normal to the boundary, $\boldsymbol{B}_g=\boldsymbol{g}\cdot\lambda$ a reduced reciprocal latice vector, and τ is the difference between the normal components of the vacuum wave vector $\boldsymbol{S}_e$ and the crystal wave vector $\boldsymbol{S}_0$. The wave vectors in the crystal are

$$\boldsymbol{S}_0=\boldsymbol{S}_e+\tau\cdot\boldsymbol{N}_e\,, \qquad (2\,\mathrm{a})$$

$$\boldsymbol{S}_g=\boldsymbol{S}_0+\boldsymbol{B}_g\,. \qquad (2\,\mathrm{b})$$

Now we introduce the excitation error ϱ_g which is in our notation

$$\varrho_g=\tfrac{1}{2}(1-(\boldsymbol{S}_e+\boldsymbol{B}_g)^2)\approx|\boldsymbol{S}_e|-|\boldsymbol{S}_e+\boldsymbol{B}_g|\,. \quad (3)$$

This excitation error ϱ_g is related to the common expression x used e. g. by Howie and Whelan [10] (or $W=x$, respectively, by Watanabe, Fukuhara and Kohra [18]) by $\varrho_g=x\cdot\varphi_g$. Using (2 a, b) and (3) we obtain

$$1+\varphi_0-\boldsymbol{S}_g^2=\varphi_0+2\,\varrho_g-\tau(2\,\beta_{ge}+\tau)\equiv D_g \quad (4)$$

with $\beta_{ge}=(\boldsymbol{S}_e+\boldsymbol{B}_g)\cdot\boldsymbol{N}_e$.

The infinite system of Eqs. (1) can be reduced to a system of n equations, if the geometrical conditions are such that only a finite number of interferences is excited. The results of our investigations will show that this treatment is correct. In the Laue case Eq. (4) can be simplified by neglecting τ^2 against $2\,\tau\,\beta_{ge}$. Inserting (4) in (1) Bethe's equations can be written in matrix form:

$$\begin{pmatrix} & \cdot & \cdot & \cdot & \\ & \cdot & \cdot & \cdot & \\ \cdot\;\cdot & D_0 & \varphi_{-g} & \varphi_{-h} & \cdot\;\cdot \\ \cdot\;\cdot & \varphi_g & D_g & \varphi_{g-h} & \cdot\;\cdot \\ \cdot\;\cdot & \varphi_h & \varphi_{h-g} & D_h & \cdot\;\cdot \\ & \cdot & \cdot & \cdot & \\ & \cdot & \cdot & \cdot & \end{pmatrix} \begin{pmatrix} \cdot \\ \cdot \\ \psi_0 \\ \psi_g \\ \psi_h \\ \cdot \\ \cdot \end{pmatrix} = 0\,. \quad (5)$$

The system (5) has nontrivial solutions only if the coefficient determinant is zero. This condition is known as dispersion equation. Multiplying column and row by $1/\sqrt{2\,\beta_{ge}}$, where g is the index of the diagonal element of the column and row, respectively, so that the diagonal element becomes

$$(\varphi_0+2\,\varrho_g)/2\,\beta_{ge}-\tau\,,$$

we obtain an n-th order eigenvalue equation for τ.

The eigenvalues τ_i $(i=1,2,\ldots,n)$ determine the wave vectors of the partial waves in the crystal according to (2 a, b) and so they represent points on the dispersion surface. i is an index characterizing a wave field.

All waves $\psi_g^{(i)}$ that belong to one g and to different indices i are superimposed and give rise to one diffracted plane wave Ψ_{ga} when leaving a parallel-sided crystal. They are separated, however, into different plane waves when leaving a wedge-shaped crystal. In the latter case the diffraction pattern displays a fine structure and each fine structure spot represents a point on the dispersion surface.

The comparison of the experiment with a dynamical n-beam calculation is difficult because the direction $\boldsymbol{S}_e$ of the incident beam cannot be accurately determined experimentally. However, by rotating the crystal wedge while moving the photographic plate one obtains a photographical record of a section through the dispersion surface which may be easily compared with the calculation. The axis of rotation determines the section plane. By such a recording the influence of accidental excitations on an interference can be investigated. This shall be demonstrated by the well-known construction of the

[18] H. Watanabe, A. Fukuhara, and K. Kohra, J. Phys. Soc. Japan **17**, Suppl. B-II, 195 [1962].

dispersion surface [19] in Fig. 2. Here we see schematically the branches of the dispersion surface belonging only to systematic interactions. The Brillouin

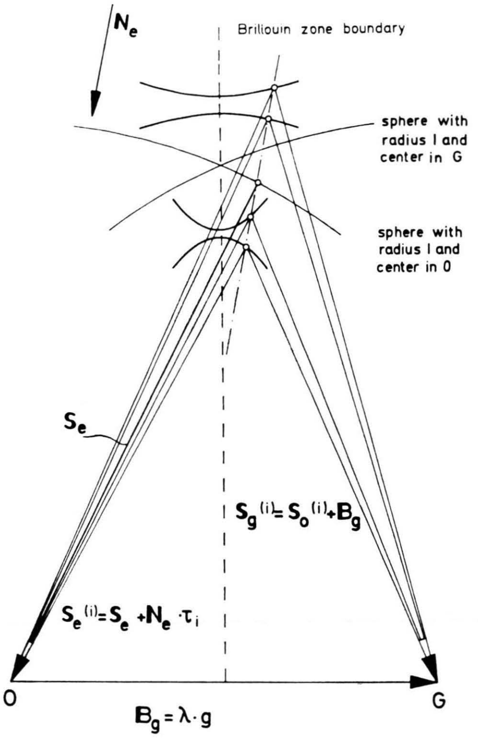

Fig. 2. Construction of the crystal wave vectors by means of the dispersion surface. Four branches of the dispersion surface are plotted.

zone boundary is perpendicular to the drawing plane. If we rotate the crystal about the axis $O \dots G$ the excitation error for G remains constant. The crystal rotation is equivalent to a rotation of the vector $\boldsymbol{S}_e$ about the axis $O\,G$ as can be seen in Fig. 3. $\boldsymbol{S}_e$ generates a cone. We erect an oblique cylinder whose basis coincides with that of the cone and whose axis is parallel to $\boldsymbol{N}_e$. Now it is easy to construct the diffraction pattern from a crystal wedge. On the exit surface the continuity of the tangential components of the wave vectors is again required by the boundary condition. The intersection of the cylinder with the dispersion surface is projected in the direction of $\boldsymbol{N}_a$ – the unit vector normal to the exit surface – onto the spheres with radius $|\boldsymbol{S}_{ga}| = 1$ surrounding the reciprocal lattice points O, G, etc. This fact can be analytically expressed by projecting the wave vector [7]

$$\boldsymbol{S}_{ga}^{(i)} = \boldsymbol{S}_e + \boldsymbol{B}_g + \varrho_g \cdot \frac{\boldsymbol{N}_a}{\beta_{ga}} + \tau_i \beta_{ge} \left(\frac{\boldsymbol{N}_e}{\beta_{ge}} - \frac{\boldsymbol{N}_a}{\beta_{ga}} \right) \qquad (6)$$

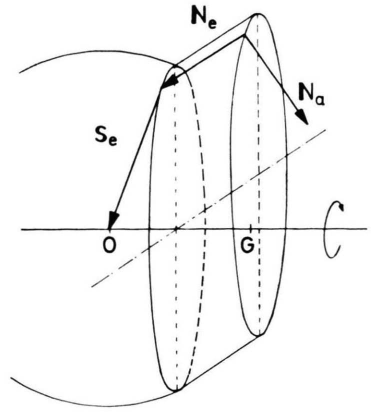

Fig. 3. Schematic diagram to show the oblique cylinder generated by $_e$ the intersection of which with the dispersion surface (not drawn) is recorded in a rotating crystal experiment. Only the sphere with radius 1 surrounding 0 is drawn.

onto the photographic plate. $\boldsymbol{S}_{ga}^{(i)}$ is the normalized vacuum wave vector of the wave that leaves the crystal (with $|\boldsymbol{S}_{ga}^{(i)}| = 1$), β_{ge} and β_{ga} are the projections of $\boldsymbol{S}_e + \boldsymbol{B}_g$ onto the normal of entrance and exit surface, respectively. These projections are recorded in a rotating crystal diagram when the photographic plate is moved simultaneously with the rotation.

In order to compare the experiment with theory one has to calculate the intensities on the branches of the dispersion surface for each reflection. This can be done quite simply with a standard computer program solving an eigenvalue problem. Once the eigenvalues and eigenvectors for a given matrix are obtained the boundary conditions can be used to determine the amplitudes of the partial waves. In a first test the influence of accidental excitations on the 002 interference of MgO was investigated by recording a section through the dispersion surface near the $[\bar{1}10]$ zone axis.

Experiment

The investigations were done with a MgO single crystal. The wedge – formed by two adjacent (100) faces – was obtained by cleaving. The crystal was mounted on a specimen holder which allowed a very precise adjustment with respect to the electron beam [20]. During small rotations, the movement of the crystal in a direction perpendicular to the beam

[19] N. Kato, J. Phys. Soc. Japan **7**, 397 [1952].

[20] G. Lehmpfuhl, Doctorate Thesis, Freie Universität Berlin 1960.

G. Lehmpfuhl and A. Reissland, *Photographical Record of the Dispersion Surface in Rotating Crystal Electron Diffraction Pattern (S. 544).*

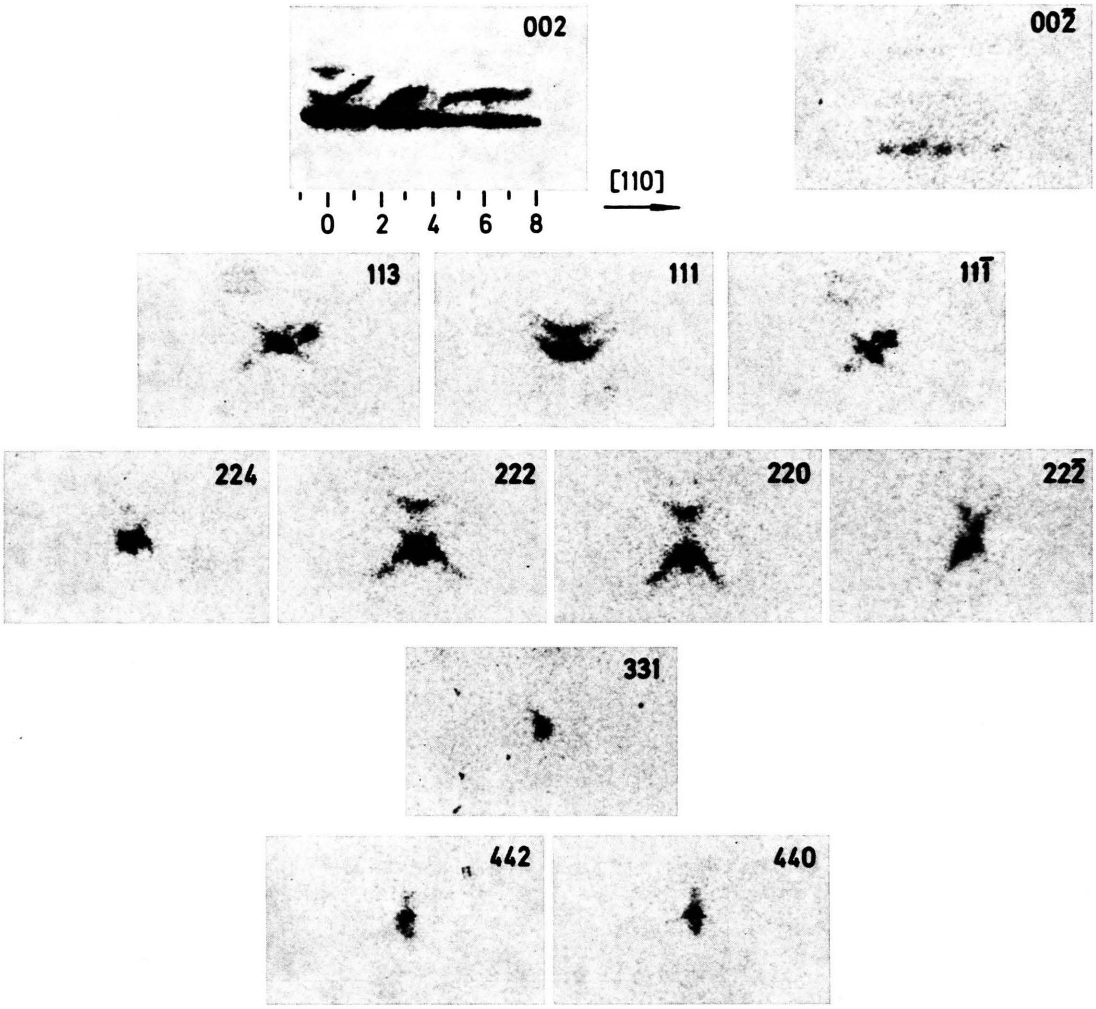

Fig. 6. Photographic record of a section through the dispersion surface in different reflections. Energy of the electrons: 60.3 keV, excitation error $\varrho_{002} \approx 0$ through the whole rotation.

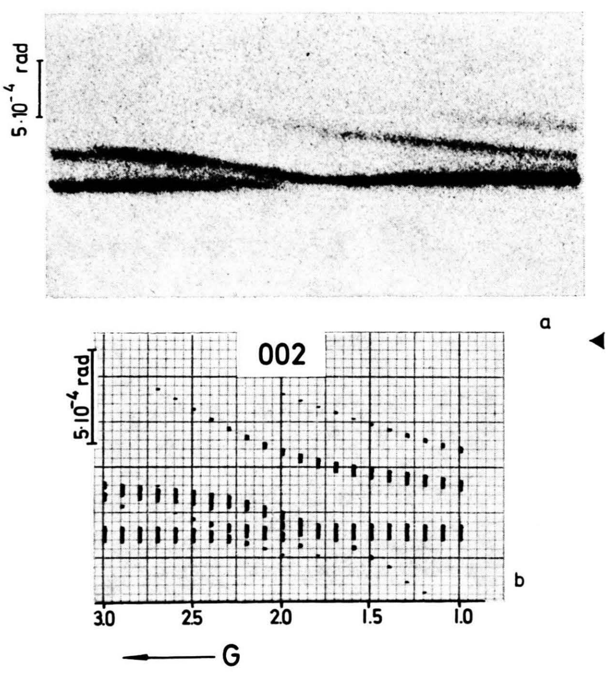

Fig. 8. a) Branches of the dispersion surface recorded in the 002 interference. The crystal was rotated manually to increase the resolution. Energy of the electrons: 60.3 keV. b) Calculated intensities on the branches of the dispersion surface considering the interaction of 17 beams. The length of the rectangles is proportional to the amplitude of the partial wave. Only the branches with intensities exceeding a lower limit are plotted, just as in the following Figs. 9 c, 10 b, 11 b, 12 b.

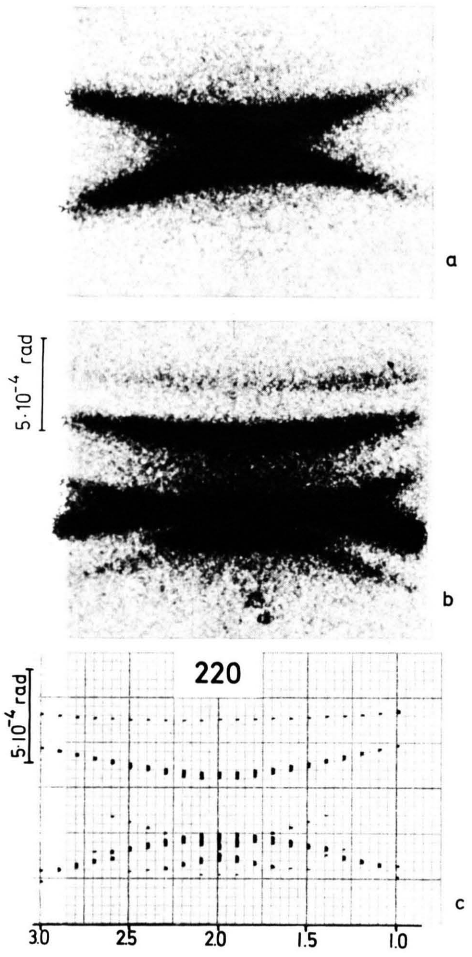

Fig. 9.

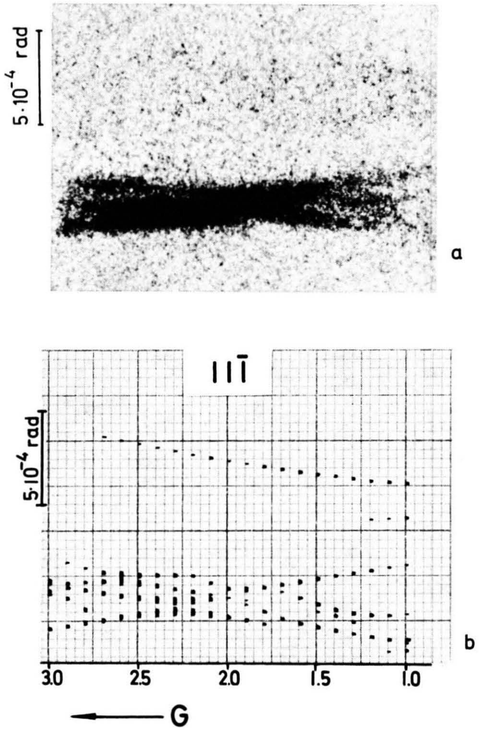

Fig. 10.

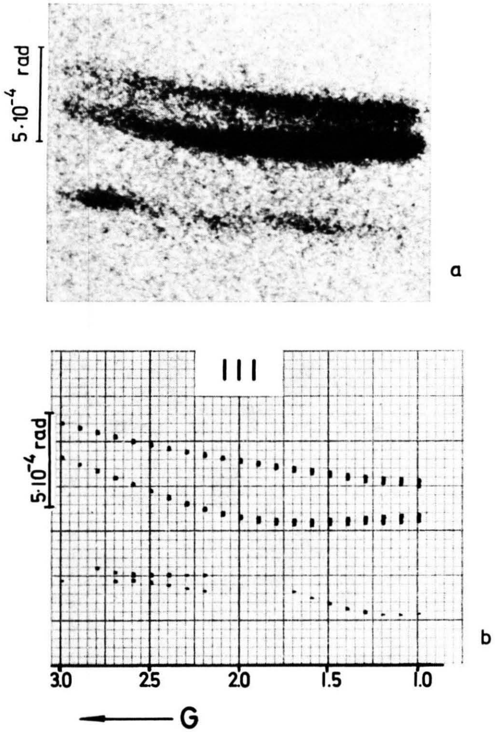

Fig. 11.

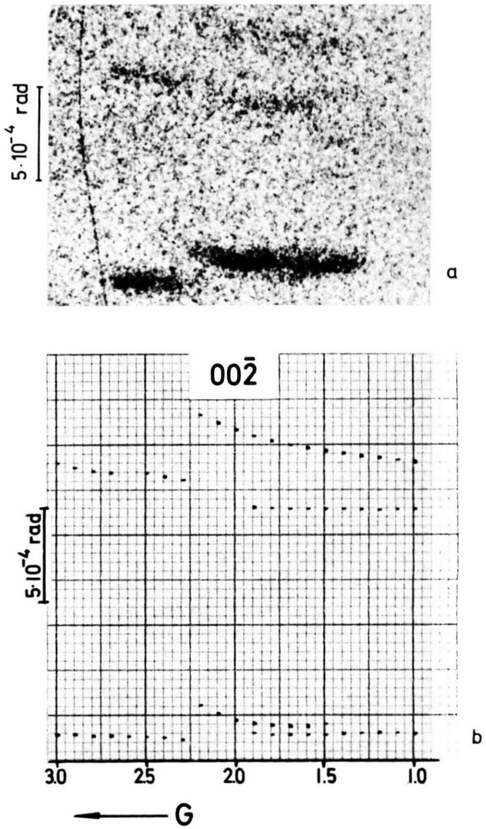

Fig. 12.

Fig. 9. Branches of the dispersion surface recorded in the 220 interference. a. Far away from the [$\bar{1}$10] zone axis under experimental conditions where the two beam approximation is satisfied. b. Near the [$\bar{1}$10] zone axis with excitation error $\varrho_{002} \approx 0$ the crystal was rotated manually to increase the resolution. c. Calculated intensity distribution on the branches of the dispersion surfaces projected in 220 direction. The length of the rectangle is proportional to the amplitude of the partial wave.

Fig. 10. Branches of the diserpsion surface: a) recorded in the 11$\bar{1}$ interference, b) calculated intensities.

Fig. 11. Branches of the diserpsion surface: a) recorded in the 111 interference, b) calculated intensities.

Fig. 12. Branches of the dispersion surface: a) recorded in the 00$\bar{2}$ interference, b) calculated intensities.

was less than $\pm 0.5\ \mu$. Fig. 4 shows the schematic diagram of the experiment. The electron beam could be focussed in the plane of the specimen with a focus diameter of $2\ \mu$ or on the photographic plate with a diameter of $10-12\ \mu$. The smallest aperture of illumination was $\alpha \approx 1.5 \cdot 10^{-5}$ rad. The crystal was ad-

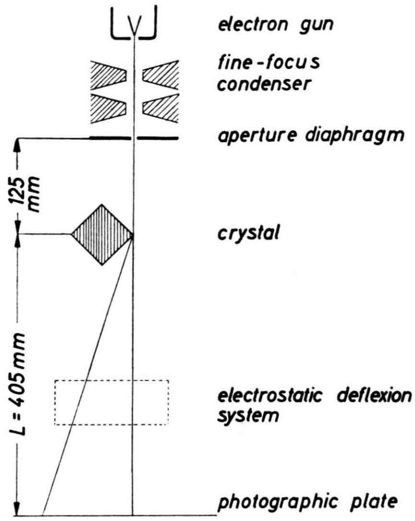

Fig. 4. Schematic diagram of the rotating crystal experiment.

justed so that the 002 interference was excited and then rotated by a synchronous motor with a drive allowing different speeds from 5.0 to 1.0 degrees per minute about the [001] axis perpendicular to the plane of drawing. Instead of moving the photographic plate, the whole diffraction pattern was deflected by an electrostatic deflecting system in the [001] direction. For a single scan, a deflecting time up to 50 seconds was used. The 002 interference remained excited with excitation error zero or nearly zero during rotation and only the accidental excitations changed. These conditions are demonstrated in Fig. 5. We see the intersection of the Ewald sphere with the $(\bar{1}10)$ plane of the reciprocal lattice. The intersection point G with the [110] axis indicates the conditions for accidental interactions. $G=2$, for instance, means that the Ewald sphere goes through the 220 reciprocal lattice point. The excitation conditions for all beams can be expressed by G and the excitation error of 002. The crystal is rotated about the [001] axis and so the systematic interactions from all reflections lying on the line through 000

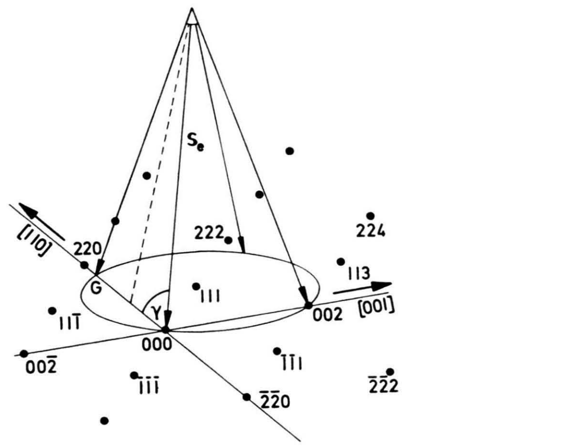

Fig. 5. Intersection of the Ewald sphere with the $(\bar{1}10)$ plane of the reciprocal lattice to demonstrate the n-beam situation. The intersection point of the Ewald sphere with the [110] axis is called G. The distance from the origin to G, measured in units $|\boldsymbol{B}_{110}| = \sqrt{2} \cdot \lambda/a$, is also called G. Since $|\boldsymbol{S}_e| = 1$ we find from the diagram in this scale $\frac{1}{2}\, G \cdot \sqrt{2} \cdot \lambda/a = \cos\gamma$ and that is equal to the projection of $\boldsymbol{S}_e$ on the [110] axis. With Eq. (A 1) from the appendix follows Eq. (A 5). G is determined by the direction $\boldsymbol{S}_e$ of the incident beam.

and 002 as $00\bar{2}$, 004 etc. remain constant. Thus the influence of systematic interactions cannot be revealed. In Fig. 6 we see the photographic record of a section through the dispersion surface in different reflections with 60.3 kV electrons. The scale indicates the intersection points of the Ewald sphere with the [110] axis. The position of the scale was determined by taking Kikuchi patterns before and after the rotation. As the excitation error ϱ_{002} stayed nearly zero the 002 reflection was recorded over the whole time whereas the other excited beams arose only in their corresponding phase of rotation. On the pattern one recognizes the influence of the accidental interactions on the shape of the dispersion surface. At $G=2$, the interaction of 220 and 222 is very strong. 440 and 442 together with $\bar{2}22$ and 224 become strong at $G=4$. One can also see a deformation of the dispersion surface where $G=8$.

Results

The photographs of the dispersion surface in different reflections were compared with n-beam calculations. These were done with an ICT 1909 in a similar way as Howie and Whelan [10] have shown using standard matrix methods. The eigenvalues and eigenvectors were calculated by the Jacobi method (Ralston and Wilf) [21]. 17-beam interactions were

* Figs. 6 – 12 on p. 546 a, b.

[21] A. Ralston and H. Wilf, Mathematical Methods for Digital Computers, John Wiley & Sons, Inc., New York 1960.

considered for 21 different directions of the primary beam. As mentioned above, the excitation conditions for all beams can be expressed by G and the excitation error of 002. From Fig. 5 we see that the excitation error is

$$\varrho_{hhl} = \left(\frac{\lambda}{a}\right)^2 (G\,h - h^2 - \tfrac{1}{2}(l^2 - 2\,l)) + \frac{l}{2}\,\varrho_{002}\,.$$

The calculations were done for $G = 1 + n \cdot 0.1$, $n = 0, 1, \ldots, 20$, and $\varrho_{002} = 0$. The computer delivered the eigenvalues τ_i and the amplitudes of the crystal waves $\psi_g^{(i)}$. In order to compare with experiment one has to consider the projection of $\boldsymbol{S}_{ga}^{(i)}$ from Eq. (6) on the photographic plate which is perpendicular to $\boldsymbol{S}_e$. This is equivalent to the multiplication of $\boldsymbol{S}_{ga}^{(i)}$ by a vector $\boldsymbol{A}$ derived in the appendix.

In the calculation we used the structure potentials for ionized Mg and O determined by TOGAWA, TOKONAMI [22] and confirmed for 200 by GOODMAN and LEHMPFUHL [11]. The energy of the electrons was 60.3 keV. We considered the interaction of the 17 beams: $\bar{1}\bar{1}\bar{1}$, $\bar{1}\bar{1}1$, $\bar{1}\bar{1}3$; $00\bar{2}$, 000, 002, 004; $11\bar{1}$, 111, 113; $22\bar{2}$, 220, 222, 224; $33\bar{1}$, 331, 333. In Fig. 7 we show the plotter curve of the eigenvalues for different G values. This is a projection of the section through 17 branches of the dispersion surface. With these eigenvalues the intensities on the branches in different reflections were calculated. They can be compared with the experimental curves.

The projected region of the intersection with the dispersion surface was expanded by decreasing the rotation speed of the crystal so that G went from 1 to 3. In Fig. 8 a we show the photographical record in the 002 interference; the excitation error ϱ_{002} was always zero. In 8 b the calculated intensities exceeding a lower limit are plotted. The length of the rectangles indicates the square root of the intensities while their center determines the position. In the region $G \approx 2$ the influence of 220 can be seen, at $G \approx 2.5$ the influence of 113 and $11\bar{1}$, and on the calculated curve at $G \approx 3.0$ the influence of 331. Without accidental interactions one should expect two parallel lines having the same intensity. The exact coordination of photograph and calculation is complicated, because this pattern was obtained by rotating the crystal manually to avoid vibrations due to the motor and to increase the resolution.

[22] S. TOGAWA, J. Phys. Soc. Japan **20**, 742 [1964]. — M. TOKONAMI, to be published.

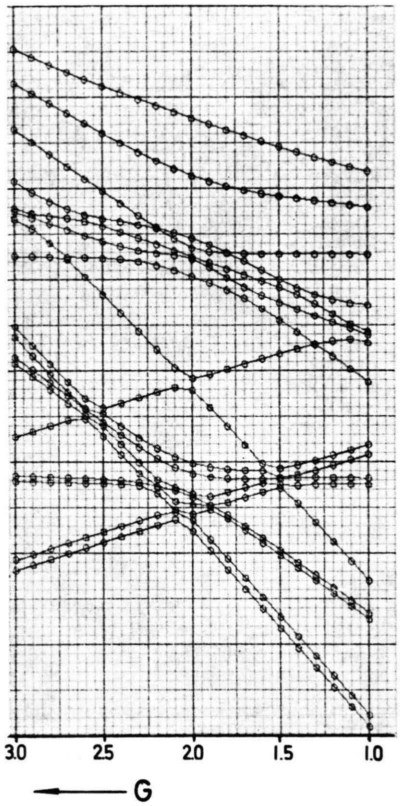

Fig. 7. Eigenvalues of a 17-beam calculation in arbitrary units for different directions of the primary beam with excitation error $\varrho_{002} = 0$. Energy of the electrons: 60.3 keV. In the calculation structure potentials for Mg^{++} and O^{--} determined by TOKONAMI, TOGAWA [22] were used.

The differences of the intensities between experiment and calculation are probably caused by the absorption and especially the anomalous absorption.

In Fig. 9 b the 220 reflection is recorded. We see a very good agreement between calculation 9 c and experiment. 9 a shows a section through the dispersion surface in a region far away from the $[\bar{1}10]$ zone axis without accidental interactions. That is the shape of the dispersion surface expected from a two beam approximation.

In Figs. 10, 11 and 12 the photographical records in the $11\bar{1}$, 111 and $00\bar{2}$ reflections are shown. There is a qualitative agreement between experiment and calculation.

Remarkably, the results of an 8-beam calculation were found in good agreement with experiment as far as the strong beams 002 and 220 are concerned. For the weak beams, however, especially for $00\bar{2}$ at $G \approx 1.5$ and 2.2, the 17-beam calculation was necessary.

Summary

A photographical record of a section through the dispersion surface shows the influence of accidental interactions on a strongly excited interference. Such a diagram reveals the limits of interpretation of a diffraction pattern by the two-beam approximation. Now we understand that the determination of the absorption from half width measurement [23] applying a two-beam approximation can be disturbed by weak branches of the dispersion surface of a many-beam system.

We found that the profile of the section through the dispersion surface is not very sensitive to the structure potentials, which are chosen for the calculation. Indeed, there are very few characteristic features in the profile of the 220 interference depending on the structure potentials. For a full analysis, however, we have to introduce the absorption in a many-beam calculation.

Our thank is due to Prof. Dr. K. Molière for his encouragement to this work. We wish to thank Dr. K. Kambe and Mr. P. Goodman for many stimulating discussions. Thanks for assistance are also due to Mr. H.-J. Krauss for programming and Mr. E. Schumann for construction of the apparatus.

Appendix

The projections of the wave vector $\boldsymbol{S}_e$ of the incident vacuum wave in the directions of the cubic axes are

$$\beta_{0i} = \boldsymbol{S}_e \cdot \boldsymbol{a}_i^{(0)} \quad , \quad i = 1, 2, 3 \; . \qquad \text{(A 1)}$$

$\boldsymbol{a}_i^{(0)}$ are unit vectors in the directions of the cubic axis. The reduced reciprocal lattice vector

$$\boldsymbol{B}_{hkl} = \lambda \cdot \boldsymbol{b}_{hkl}$$

is for a cubic crystal with lattice constant a

$$\boldsymbol{B}_{hkl} = (\lambda/a)\,(h\,\boldsymbol{b}_1^{(0)} + k\,\boldsymbol{b}_2^{(0)} + l\,\boldsymbol{b}_3^{(0)}) \quad \text{with} \quad \boldsymbol{b}_i^{(0)} \cdot \boldsymbol{a}_j^{(0)} = \delta_{ij} \, . \qquad \text{(A 2)}$$

With these β_{0i} and $\boldsymbol{B}_{hkl}$ the excitation error ϱ_{hkl} according to Eq. (3) can be expressed as

$$\begin{aligned} \varrho_{hkl} &= -\boldsymbol{S}_e \cdot \boldsymbol{B}_{hkl} - \tfrac{1}{2}\,\boldsymbol{B}_{hkl}^2 \\ &= -(\lambda/a)\,(h\,\beta_{01} + k\,\beta_{02} + l\,\beta_{03}) \\ &\quad - \tfrac{1}{2}(\lambda/a)^2 (h^2 + k^2 + l^2) \, . \end{aligned} \qquad \text{(A 3)}$$

Considering the $(\bar{1}10)$ plane of the reciprocal lattice one can replace the β_{0i} by the excitation errors ϱ_{220} and ϱ_{002} and obtains for $h = k$

$$\begin{aligned} \varrho_{hkl} = \tfrac{1}{2}[&h\,\varrho_{220} + l\,\varrho_{002} \\ &+ (\lambda/a)^2 (4\,h - 2\,h^2 + 2\,l - l^2)] \, . \end{aligned} \qquad \text{(A 4)}$$

Instead of ϱ_{220} we may introduce the intersection G of the Ewald sphere with the [110] axis. According to Fig. 5 we find

$$(\lambda/a)\,G = -(\beta_{01} + \beta_{02}) \, . \qquad \text{(A 5)}$$

On the other hand, the β_{0i} can be expressed by ϱ_{220} (or G) and ϱ_{002}.

In the diffraction pattern the projection of the wave vector $\boldsymbol{S}_{ga}^{(\;)}$ according to Eq. (6) is recorded. We have to find a unit vector $\boldsymbol{A}$ perpendicular to $\boldsymbol{S}_e$ and the edge [001] of the crystal, that means $\boldsymbol{A} \cdot \boldsymbol{S}_e = 0$ and $\boldsymbol{A} \cdot [001] = 0$. This vector is

$$\boldsymbol{A} = -\frac{\beta_{02}}{\sqrt{1-\beta_{03}^2}} \cdot \boldsymbol{a}_1^{(0)} + \frac{\beta_{01}}{\sqrt{1-\beta_{03}^2}} \cdot \boldsymbol{a}_2^{(0)} \, . \qquad \text{(A 6)}$$

Multiplying (A 6) by (6) with $\boldsymbol{N}_e = -\boldsymbol{a}_2^{(0)}$ and $\boldsymbol{N}_a = \boldsymbol{a}_1^{(0)}$ one obtains the positions of the diffracted beams on the photographic plate.

[23] G. Lehmpfuhl and K. Molière, J. Phys. Soc. Japan **17**, Suppl. B-II, 130 [1962].